Universidade do Minho
Escola de Engenharia

Joaquim André Moreira Maia

Preprocessing Non Organic Objects in Computer Tomography Images

Outubro de 2010

Universidade do Minho
Escola de Engenharia

Joaquim André Moreira Maia

Preprocessing Non Organic Objects in Computer Tomography Images

Mestrado de Informática

Trabalho efectuado sob a orientação do
Professor Doutor Luís Paulo Santos
e da
Doutora Céline Paloc

Outubro de 2010

Universidade do Minho, ___ /___ /_____

Assinatura: _____

Acknowledgments

I would like to thank Luís Paulo Santos, my coordinator from University of Minho, for the given support and for making possible to develop my work in VicomTech. And I would like to thank Julián Flórez Esnal and Jorge Posada for giving me the opportunity to develop this work in VicomTech (Visual Interaction Communication Techniques), using the institute financial and logistic support.

I am grateful for the close support and guidance that was given to me by Luis Kabongo, from VicomTech. I also would like to thank all my lab colleagues. The discussion and sharing of knowledge among us helped me a lot in my research work. I would also like to thank Céline Paloc for putting at my disposal all the resources, both human and logistic, so that my work could be accomplished successfully.

Preprocessing Non Organic Objects in Computer Tomography Images

Abstract

The latest developments in the use of digital medical images and the ever increasing processing power of current computers result in a constant increase on the amount of medical images created every day. A traditional Computed Tomography scan of a part of the body gives us a set of 2D images which, in addition to the relevant anatomical information, may contain other type of information, like the bed where the patient is lying, metal objects or even scanning information engraved in the image. This type of undesired information is normally ignored by the radiologist when visualizing slice by slice, but it can lead to the occlusion of some parts of the body when dealing with 3D visualization and also increases considerably the processing time of associated algorithms, like volume or surface rendering. Metal artifacts are a major problem in computed tomography because they can cause large areas of signal void and extensive distortion around the implant leading to a corrupted 3D visualization. In addition to this, the presence of this non anatomical information harms the data storage by requiring more disk space than just the relevant anatomical information. This thesis proposes and evaluates two implementations, based on image processing, which deal with the non anatomical objects and metal artifact problematic.

Pré-processamento de Objectos Não Orgânicos em Imagens de Tomografia Computadorizada

Resumo

Os últimos desenvolvimentos na utilização de imagens médicas digitais aliada ao aumento da capacidade de processamento provocaram um aumento significativo das imagens médicas que são criadas todos os dias. Da aquisição de uma parte do corpo através de tomografia computadorizada obtêm-se um conjunto de imagens 2D que, para além de representar a informação anatómica, pode conter outros tipos de informação como a cama onde o paciente se deita, objectos metálicos ou ainda outro tipo informação gravada na imagem. Este tipo de informação é normalmente ignorada por radiologistas a quando da sua visualização por camadas 2D, contudo pode provocar oclusões em algumas partes do corpo em visualizações 3D e ainda implicar um aumento de processamento significativo dos algoritmos associados, como volume ou surface rendering. Artefactos metálicos são um problema em tomografia computadorizada pois estes podem causar amplas áreas de sinal corrompido e distorções à volta do implante resultando numa visualização 3D corrupta. Além disso, a presença deste tipo de informação não anatómica prejudica a politica de armazenamento de dados exigindo mais espaço em disco. Esta tese propõe e avalia duas implementações, baseadas em processamento de imagem, para lidar com a problemática dos artefactos metálicos e de objectos não anatómicos.

Contents

1 Introduction

With the evolution in processing capacity, the last years have seen tremendous advances in medical technology to acquire data about the human body with ever increasing resolution, quality and accuracy. Medical visualization deals with the analysis, visualization, and exploration of medical image data. It covers several applications areas like education, diagnosis and treatment planning.

The data, on which medical visualization methods and applications are based, is acquired with radiological scanning devices such as Computed Tomography (CT) and Magnetic Resonance Imaging (MRI). Although other imaging modalities such as 3D Ultrasound, Positron Emission Tomography (PET) and imaging techniques from nuclear medicine are available, CT and MRI dominate due to their high resolution and their good signal-to-noise ratio. Computer Tomography x-ray images still play a crucial role in diagnosis and surgery or therapy planning. Radiologists, for instance, keep using 2D images (volume slices) for diagnosis and treatment planning from 3D modalities such as Computerized Tomography or Magnetic Resonance Imaging. So slice-by-slice inspection of medical volume data is still a common practice[10].

These datasets may be visualized in three dimensions, in order to facilitate the interpretation for the specialists. 3D visualization of organs and internal patient structure offers another type of spatial representation that can be very helpful due to a better spatial localization and orientation, tissue differentiation, etc. However, other objects acquired during the scanning process or even scanning information engraved in the image may interfere in the final visualization causing deterioration in the final view for the user. Two possible types of objects can be considered: inside a organic area or outside organic area.

Objects inside a organic area are, usually, metal implants which can lead to a significant deterioration of the image in these regions leading to a wrong or impossible interpretation.

Objects outside organic area typically do not have a classification because patients are advised to remove, in an earlier stage, objects that may cause deterioration in the image. However, elements such as the bed where the patient is lying, clothing or other non biological objects may be present. While these are easily ignored by a radiologist on traditional 2D images, they can have a major impact in the visualization of the 3D volume because they can occlude visibility when performing 3D rendering and rise up the rendering time. In addition to this, the presence of this non anatomical information harms data storage by requiring more disk space than just the relevant anatomical information.

The aim of the thesis is to propose new techniques of image processing to provide a significant improvement in the 3D visualization of medical CT images by removing the above referred objects. This document describes some computer tomography essentials and two techniques which aim to provide a better 3D visualization or reconstruction. In the next section, the theory of Computer Tomography and some base knowledge about standards on medical image are discussed. An historical perspective is also presented. Section 3 is about artifact reduction inside a organic area, specifically Metal Artifact Reduction on Teeth. Some bases about this particular region are presented and the most important State of Art is detailed. Non Organic Object Removal concepts and similar works are presented in Section 4.

2 Theoretical Concepts

2.1 Computer tomography

Computer tomography is a medical imaging method where digital geometry processing is used in order to generate a three dimensional image of the internals of an object from a large series of two dimensional X-ray images taken by rapid rotation of the X-ray tube 360° around the patient. It is the preferred modality for cancer, pneumonia, and abnormal chest x-rays. CT is far superior from others medical imaging methods, like MRI, for visualizing the lungs, organs in the chest cavity between the lungs and organ tear/injury are quickly and efficiently represented.

The first CT scanner was developed by *Sir Godfrey Hounsfield* originally known as "EMI scan" [16]. CT scanning has become an essential radiological technique applicable in a wide range of diagnostic clinical situations: head, neck, thorax, urogenital tract, abdomen and musculoskeleton system [35].

He has presented a standardized unit, which represents an affine line transformation, for reporting and display reconstructed X-ray CT values.

In modern CT-scanners devices, images have 512x512 pixels representing the CT-number which is expressed in *Hounsfield Units (HU).* The CT-number is defined as:

$$CT - Number(HU) = \frac{u - u_{H2O}}{u_{H2O}}.1000 \tag{1}$$

where u is the linear attenuation coefficient and H_{2O} is the linear attenuation coefficient for water. He defined as well the CT-number for air, water and bone(Figure 1).

The use of this standardized scale facilitates the inter-comparison of CT values obtained from different CT scanners and with different X-ray beams energy spectra, allowing conversions for tissue detection between the different

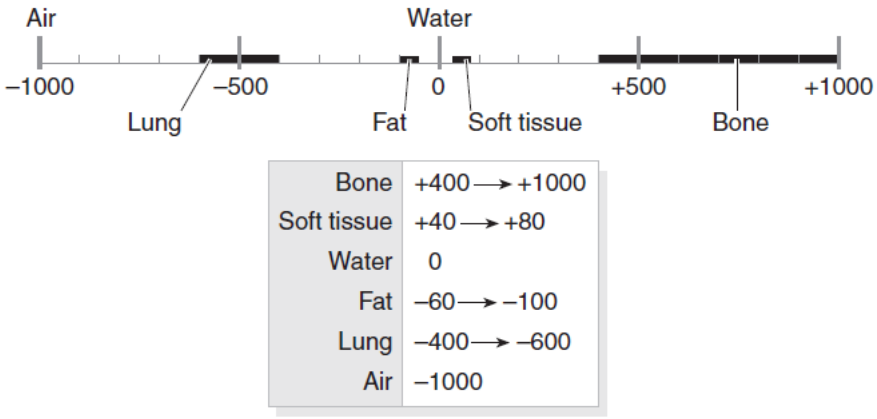

Figure 1: The Hounsfield scale of CT numbers.

data types of an image. This scale assigns air and water to a CT number of, respectively, −1000 *HU* and 0 *HU* [35]. The range of CT numbers is 2000 *HU* wide although some modern scanners have a greater range of *HU* up to 4000.

2.1.1 Basic Steps in CT Image Acquisition

In order to understand certain aspects that will be presented at a later stage it is essential to know some aspects of how the CT data set is constructed. CT image acquisition is not a trivial subject and in order to not leave the central subject of the thesis, the basic steps performed by the scanner to obtain the final data set are presented in a simple way.

X-ray slice data is generated using an X-ray source that rotates around the object; X-ray sensors are positioned on the opposite side of the circle from the X-ray source. Many data scans, projections, are progressively taken as the object is gradually passed through the gantry. After a sinogram image (Figure 2) is obtained by stacking the projections. Finally, a discrete version of the inverse *Radon* transform is applied(e.g. *Filtered backprojection*) in order to convert the sinogram to the final data set.

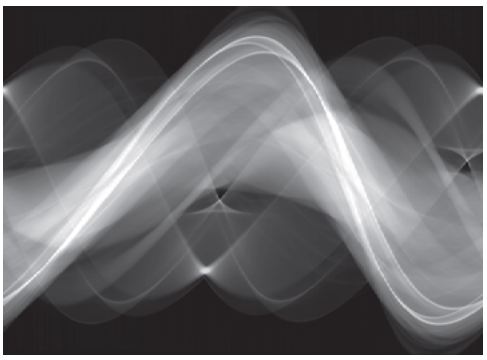

Figure 2: A sinogram 2D data set example

2.1.2 Artifacts in CT

Although CT is a relatively accurate test, it is liable to produce artifacts. The term *artifact* is applied to any systematic discrepancy between the CT numbers in the reconstructed image and the true attenuation coefficients of the object[4].

It's common to have some noise in CT images that are provoked by some artifacts that can be divided in four major categories[4]:

- **Physics-based artifacts**: resulting from the physical process involved in the acquisition of CT data.
- **Patient-based artifacts**: caused by factors as patient movement or the presence of metallic materials in or on the patient.
- **Scanner-based artifacts**: imperfections in the scanner function.
- **Helical and multisection artifacts**: produced by the image reconstruction process.

This thesis focuses on patient-based artifacts category.

The presence of metal objects in the scan field can lead to severe streaking artifacts[4]. Metal artifacts are caused by the presence of high density objects (usually made of metal), such as dental fillings, metal prosthetic devices,

surgical clip, etc. They appear as a streaking artifact on an image as seen on figure 3. The primary reason that streaks occur from metal objects is because the objects exceed the maximum attenuation value in the CT scale. Older scales assign the number +1000 as the maximum value and this value coincides with the attenuation value of cortical bone, which is primarily the densest structure in the human body. Dental fillings or prosthetic devices which are made of metal have higher attenuation values greater than cortical bone. These metallic type objects exceed the dynamic range of the detectors in the detector array causing streak artifacts.[4]

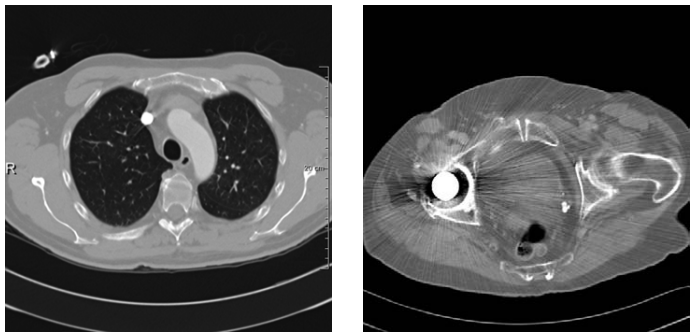

(a) (b)

Figure 3: (a) CT image without artifacts (b) CT image of a slice through the prosthesis showing streak artifacts due to the metallic implant[35].

2.1.3 The DICOM Standard

Usual image files formats (JPG, GIF, PNG, etc) only support 8-bit gray-scale and although the millions of colors that can be represented they support only 256 shades of gray. Moreover, the graphics cards that currently exist in the market are incapable of display more than 256 shades of gray on the monitor. A medical image pixel is usually stored as a 16-bit integer. Two industry standard file formats that support 16-bit data are DICOM and TIFF.

The Digital Imaging and Communications in Medicine [36] (DICOM) standard was created by the National Electrical Manufacturers Association

(NEMA) to aid the distribution and viewing of medical images, such as CT scans, MRIs, and ultrasound. DICOM is the most common standard for receiving scans from a hospital. A single DICOM file contains a header which stores patient and scan information that is needed to perform conversions between *Hounsfield* unit and the specific data type. Besides the header, the DICOM file stores also the image data. DICOM stores a wider dynamic range of information than can be displayed on a PC video monitor. This is usually resolved by compressing the 16 bit data from a user defined display range (the "window") to 8 bit (256 shades of gray.) The term *window/level* represents the central *Hounsfield* unit of all the numbers within the window width. The window width covers the HU of all the tissues of interest and these are displayed as various shades of Grey. Tissues with CT numbers outside this range are displayed as either black or white.

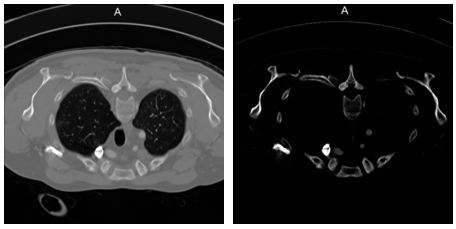

(a) (b)

Figure 4: DICOM image with differents *window/level*

2.1.4 Medical 3D Rendering Methods

Among existing rendering methods two classes of techniques are commonly used in medical visualization: surface rendering[21] and volume rendering. These techniques although well know and well documented, weren't widely used because of the cost (compute and/or preprocessing). However, in the last couple of years a new generation of workstations has brought the benefits of 3D to the clinical community at desktop prices.

1. **Surface Rendering** methods in medical data sets require a segmentation(e.g. threshold) pre-processing step to visualize the desirable areas, although multiple models can be constructed from various different thresholds, allowing different colors to represent each anatomical component such as bone, muscle, and cartilage. However, the interior structure of each element is not visible in this mode of operation. Polygons representing the outer surface of an object can be calculated using, for instance, a *Marching Cubes* [22] algorithm. The method of identifying surfaces of interest, referred to as segmentation, is generally a difficult problem for medical images.

2. **Volume Rendering** is a direct way for reconstruction of 3D structures. It represents 3D objects as a collection of building blocks know as voxels, or volume elements. A voxel is a sample of the original volume, a 3D pixel on a regular 3D grid or raster. Each voxel has associated one or more values quantifying some measured or calculated property of the original object, such as transparency, luminosity, density, flow velocity or metabolic activity. The main advantage of this type of rendering is its ability to preserve the integrity of the original data throughout the visualization process. This technique does not need a pre-processing step like surface rendering, however, requires huge amounts of computation time and is generally more expensive than conventional surface rendering .

2.2 Mathematical Morphology

Mathematical morphology describes operations based on the set theory and is widely used in noise and artifact reduction in image processing. It is based in minimum and maximum operations and depends on the size and shape of the *structuring element*[1](SE)[37]. Morphological processing has two basic operations: *dilation* and *erosion*. Many of the morphological algorithms are based in combinations of these operations.

Dilation is a morphological transformation that combines two sets using vectorial addition. With A and B as sets, the dilation of A by B is denoted by $A \oplus B$ and is defined as follows:

$$A \oplus B = \{z|(\hat{\mathrm{B}})_z \cap A \neq 0\} \tag{2}$$

where A is the image to operate, B is the second set normally called as *structuring element*, z the set if all the displacements and $\hat{\mathrm{B}}$is the reflection of set B. In a pratical way the dilation filter expands the shapes contained in the input image as is shown in the figure 5e.

[1]shape used to probe or interact with a given image with the purpose of drawing conclusions on how this shape fits or misses the shapes in the image.

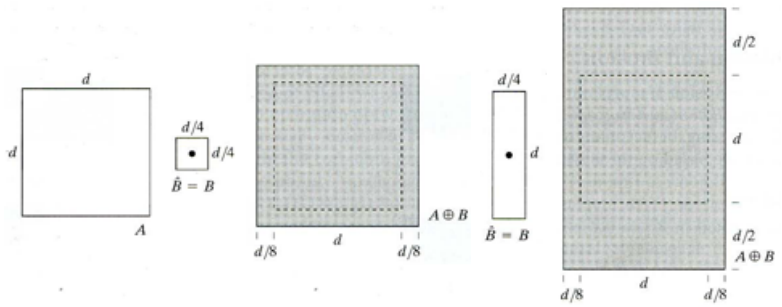

(a) (b) (c) (d) (e)

Figure 5: (a) Set A (b) Set B - *structuring element* (c) Dilation of A by B (shaded) (d) Elongated *structuring element* (e) Result of the dilatation with the previous SE - Images Source: Gonzalez and Woods[13]

Erosion basically shrinks the objects and can be viewed as a morphological transformation that combines two sets and a subtraction operation. It is denoted by $A \ominus B$ and defined as:

$$A \ominus B = \{z|(B)_z \subseteq A\} \tag{3}$$

So the erosion of A by B is the set of all points z such that B, translated by z, is contained in A.

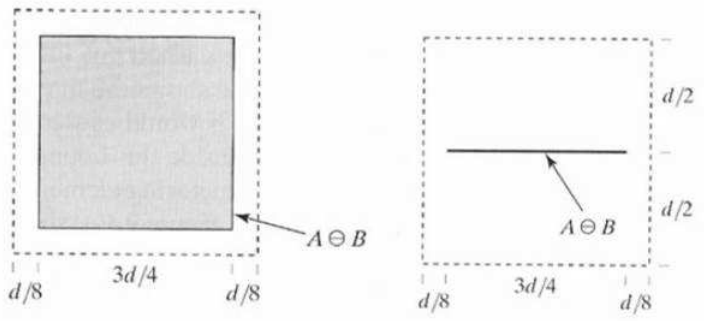

Figure 6: Example of an erosion of the previous set A with different SE's - Images Source: Gonzalez and Woods[13]

As previously mentioned it is possible to combine basic morphological operators and derive others like *opening* and *closing* with small execution times.

Opening it is a morphological operation that has the characteristic of smoothing the contour of the objects, i.e., breaks narrow isthmuses and erases thin protrusions. The *opening* of a set A by a *structuring element* B is denoted as $A \circ B$ and defined as:

$$A \circ B = (A \ominus B) \oplus B \tag{4}$$

as we can note in the formula the *opening* operation is composed by a *erosion* followed by a *dilation*.

Closing tends to smooth sections of contours, but as opposed to *opening*, fuses narrow breaks and long thin gulfs, eliminates small holes and fills gaps in the contour. It is denoted by $A \bullet B$ and defined as:

$$A \bullet B = (A \oplus B) \ominus B \tag{5}$$

therefore the *closing* operation is composed by a *dilation* followed by a *erosion*.

Figure 7 shows a set A where different morphological operations are applied with the circular *structuring element* that is presented in the second and third images. The second and the third images illustrate the erosion and opening respectively of the A by SE B. The forth and fifth images illustrate dilation and closing.

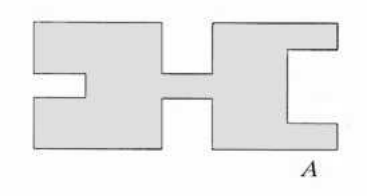

(a)

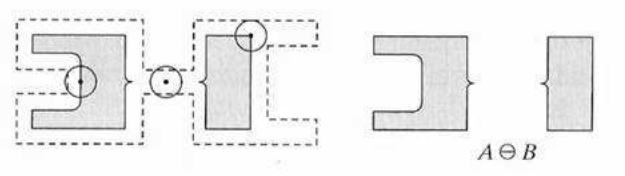

(b)

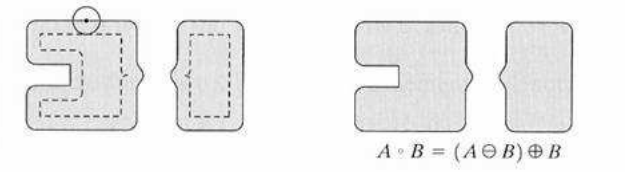

(c)

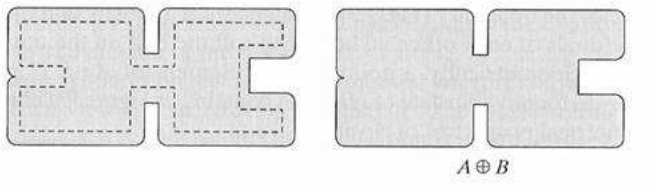

(d)

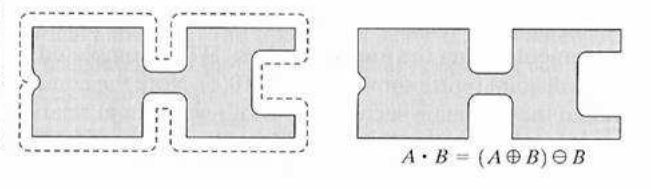

(e)

Figure 7: Examples of 4 morphological operations applied in A by an SE B. (a) Original Image (b) Erosion (c) Opening (d) Dilation (e) Closing - Images Source: Gonzalez and Woods[13]

Mathematical Morphology can be applied in specific directions using orientated SEs. Figure 8 shows the effects of an opening operation in an image using different orientated SEs. Horizontal SE's tends to erase vertical elements and vertical SE's tends horizontal elements so there is a relationship between the directions of the SE and the erased items: erased objects are perpendicular to the SE orientation[37].

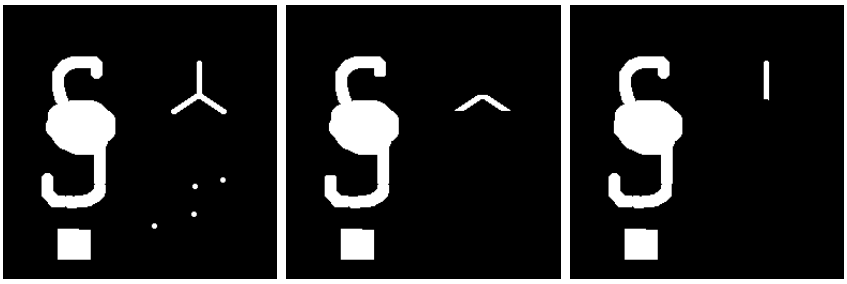

(a) (b) (c)

Figure 8: (a) Original image. (b) Opening with horizontal s.e of size=9. (c) Opening with a vertical s.e of size=9 - Images Source: Naranjo et all.[37]

With the *opening* and *closing* operations it is possible to compose other operations like the *alternating sequential filtering*(ASF).

Alternating Sequential Filter corresponds to a sequence of *opening*($\circ$) and *closing*($\bullet$) operations where the size of the structuring element increases from 2 till λ, i.e.:

$$\bullet_{B_\lambda} \circ_{B_\lambda} \bullet_{B_{\lambda-1}} \circ_{B_{\lambda-1}} \cdots \bullet_{B_2} \circ_{B_2} \tag{6}$$

These sequential filters reduce the noise, obtaining a better approximation of the noise-less signal than a simple opening and closing concatenation[37]. The processing time of the ASF filters is highly dependent of the size λ [33] .

Beside the morphological operations mentioned before there are some morphological algorithms that can calculate some properties or shapes of an image[13]. Connected Components and Region Filling are some of them.

Connected Components is an important algorithm to many automated image analysis applications that has as feature the labeling of objects. Let Y represent a connected component contained in a set A and assume that a point p of Y is know. Then the following interactive expression yields all the elements of Y:

$$X_k = (X_{k-1} \oplus B) \cap A \qquad k = 1, 2, 3, ... \tag{7}$$

where $X_0 = p$ and B is a structuring element. The algorithm converges when $X_k = X_{k-1}$.

Figure 9a shows a 2D image with two objects that will be processed with connected components. The *structuring elements* iterates the image, as it is represented in Fig. 9b and Fig. 9c, and gives a new label to a pixel if this doesn't contain any label. Fig. 9d shows the final output colored with the label information.

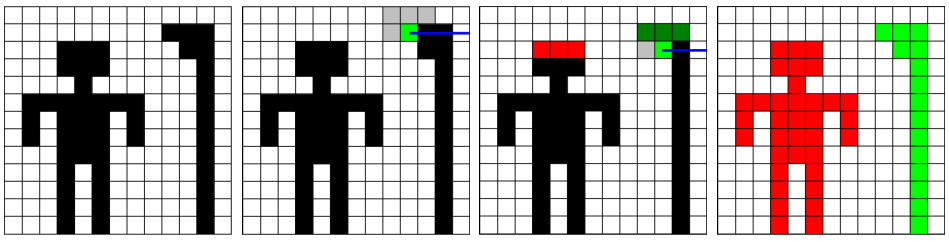

Figure 9: (a) Original image (b)(c) Iterations of the SE on the image (d) Image recolored with the label information.

Region Filling algorithm fills regions inside a set of connected boundary points and is based on a set of dilation's, complementation and intersections. Assuming that all non-boundary(background) points are labeled 0 and p labeled as 1 the following procedure fills an region with 1's:

$$X_k = (X_{k-1} \oplus B) \cap A^C \quad k = 1, 2, 3, ... \tag{8}$$

where $X_0 = p$, B is the structuring element and the algorithm terminates at iteration step k if $X_k = X_{k-1}$.

(a) (b) (c)

Figure 10: (a) Binary image (the white dot inside one of the regions is the starting point) (b) Result of filling that region (c) Final output of the region filling - Images Source: Gonzalez and Woods[13]

2.2.1 Mathematical Morphology in Polar Coordinates

The use of mathematical morphology for artifact and noise reduction in Cartesian space achieves the desired results when working with non rounded objects but when these objects are present the results achieved are not so good. It has been suggested that the image should be transformed to other domains depending of the nature of the object or the analysis that must be carried out. Polar transformation gives a better representation to analyze images which contain some kind of radial symmetry, or in general, which have "a center".

The polar coordinate system defines each point by its radial and angular coordinates denoting the distance from the pole, the origin of symmetry, and the angle determined with the polar axis[37]. Polar transformation converts an original image *(x, y)* in the Cartesian coordinates into an image in the polar coordinate *(ρ, Θ)*. More precisely, with respect to a central point (x_c, y_c):

$$p = \sqrt{(x - x_c)^2 + (y - y_c)^2}, \quad 0 \leq p \leq p_{max} \tag{9}$$

$$\Theta = arctang\left(\frac{y - y_c}{x - x_c}\right), \quad 0 \leq \Theta \leq 2\pi \tag{10}$$

Figure 11 shows an conversion between Cartesian and polar coordinates. The body center of the crab is considered as the central point (x_c, y_c).

(a) (b)

Figure 11: (a) Original image in Cartesian coordinates (b) Image converted to polar coordinates where (xc, yc) corresponds to the body center of the crab.

3 Non Anatomical Object Removal from CT Images

CT scanning of a part of the body gives us a group of images, slices, that besides the anatomical information can contain other type of information like hospital logo, text and other objects that usually appear like the bed where the patient is lying as seen in figure 12. This type of extra-information is normally ignored by the radiologist when visualizing slice by slice, but it can lead to the occlusion of some parts of the body when dealing with 3D visualization and also increases considerably the processing time of associated algorithms, like volume rendering. In addition to this, the presence of this non anatomical information harms data storage saving policies by requiring more disk space than just the relevant anatomical information.

3D rendering of organs and internal patient structure offers a better spatial representation that can be very helpful due to a better spatial localization and orientation, tissue differentiation, etc. However, other objects acquired during the scanning process, like the bed on which the patient is lying, may interfere in the final visualization. Automatic removal of such objects will thus increase significantly the usability of 3D medical imaging techniques.

3.1 Research Goal

The objective is to implement an automatic or semi-automatic method to remove multiple non anatomical objects from CT images. The automatic solution should not require any human interaction therefore can be optimal for processing of high volumes of images. Semi-automatic solution should require interactive activities such as detection of certain regions of interest but at most it should require a single interaction (slice by slice approach would be unusable). This semi-automatic solution has the objective of making the algorithm robust, able to handle significant variations in the image input, such as crops on the original image.

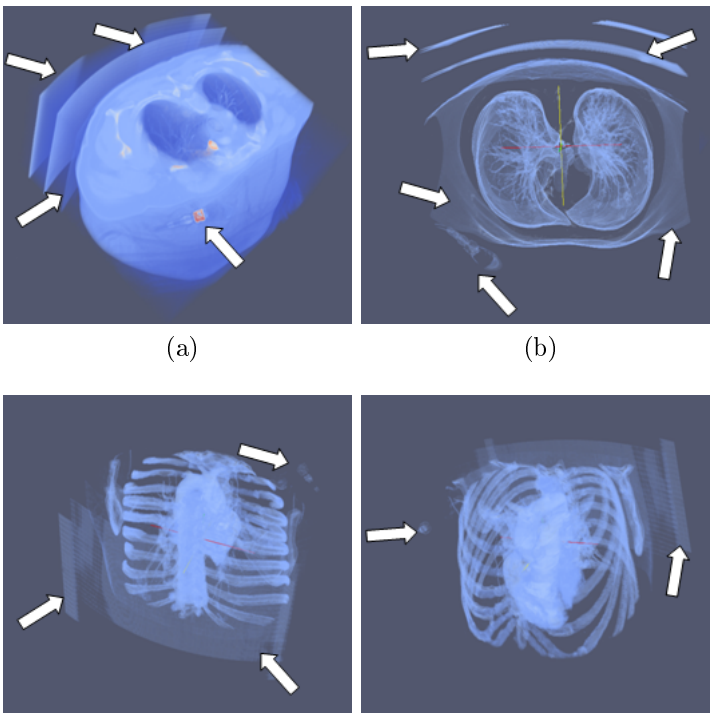

(a) (b)

(c) (d)

Figure 12: The influence of non-anatomical objects in 3D visualization.

3.2 State of the Art

Very few publications can be found in the literature about non anatomical objects removal in medical images, but two possible ways of solving this problem can be considered: Preprocessing information or filtering during visualization. Previous research is mostly based on preprocessing filtering [18, 19, 27, 26]. Live visualization filtering increases computation complexity due to conflicts like concurrent access in memory for both processing and visualization.

Bed/line removal algorithms [19, 18] consider preprocessing filtering and use a bed scan template as reference. Using this template, the original data set volume is spatially aligned and reduced. In a second step adaptive thresholding and refinements were applied to the resulting volume, which was then cropped, to exclude empty sections, thus reducing the image volume. Average results show that the volume was reduced in 41% [19] , thus causing a major improvement in the 3D visualization and in the processing time. Although having good practical results bed removal algorithms that are based in template matching are computationally expensive[6] due two distinct reasons: multiple templates are needed to cover a large variety of objects and template representation is not trivial, since they usually require high resolution, which implies heavier computational requirement. As medical imaging scanning devices vary depending on brands and models, a bed template should consist of an extensive set of known templates images, thus increasing processing complexity. Moreover, the presence of other non anatomical objects such as clothing or metal are not removed in these approaches.

Henning Müller and colleagues[27] developed an automatic solution to handle another type of non-anatomical types of information like text and logos. The first step of the implementation was to remove specific structures: grey squares and university logo. As these structures have the same position in all the images a detection algorithm was performed (thresholding and white pixel count). If the desired structure was detected, this area was filled

with a black value. Later, a median filter was utilized to remove smaller parts that could remain from the previous processing. Then an edge detection was applied, followed by a threshold, to remove structures of low intensity. Finally the image was cropped based in a bounding box algorithm. The proposed method removes the objects in question but is very specific, i.e., the same algorithm applied to other medical images in order to remove similar information (such as text and logo) will not produce the desired result and can erase some important information. For instance, if the logo in the new image has different dimensions it will not be removed completely. Moreover, if the logo is not at the same position the proposed solution may remove some undesired information.

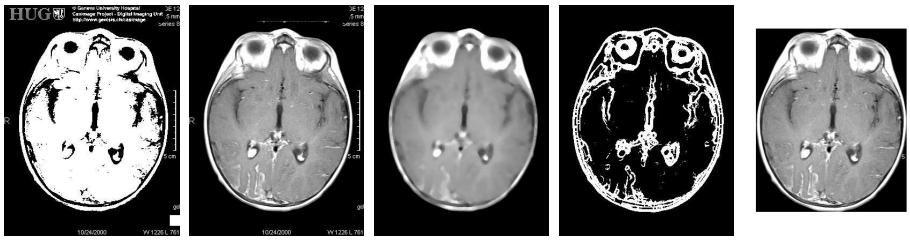

(a) (b) (c) (d) (e)

Figure 13: a) Original image b) Removal of specif structures c) Median filtering d) Edge detection + Thresholding e) Final output

3.3 Method

When a CT/MRI scan is requested by a professional it has the aim to represent information of an anatomical part (e.g. the lungs), therefore the image produced will logically contain mostly information of this area. The proposed method is based in this premise, ie, the image obtained from a scanner may contain non anatomical objects that have smaller area than the anatomical ones.

In this section a non anatomical object removal algorithm is presented, based on preprocessing filtering, that can be used in two different ways: Automatic and Semi-automatic. Both share common steps therefore the following description is based on the diagram presented on figure 14.

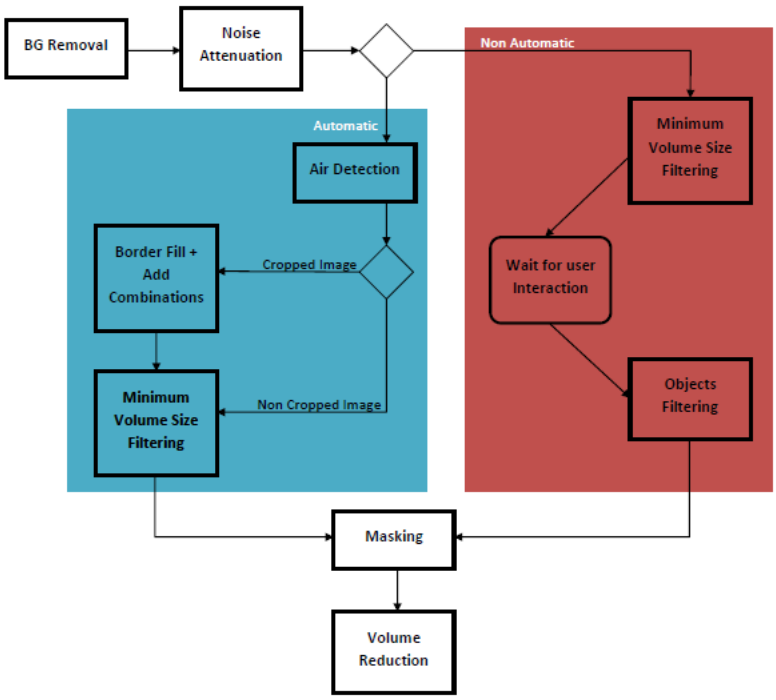

Figure 14: Block diagram of the proposed algorithm.

3.3.1 Background Removal

The aim of this step is to create a segmented volume that represents all the objects that exists. This volume is the basis for all the implementation because after the intermediary steps it will be used to create a mask of the original volume. More precisely the type of segmentation that we want to obtain is a thresholded volume that contains skin contours and logically the inside information.

Source CT data describes distribution of tissues, in *Hounsfield units* (HU), in a volume of scanned body part. Soft human tissues have densities in the range 200-400 HU[20]. These values are utilized to obtain a thresholded volume. Although some non-biological objects are excluded with this operation, most common (e.g. the bed) have similar intensities as soft human tissues therefore are represented on the thresholded image.

This preprocessing stage can be implemented in different ways, simple *Hounsfield* unit threshold segmentation or automatic threshold segmentation like *Otsu GL H* [29] can also be applied at this stage to ensure an automatic preprocessing procedure.

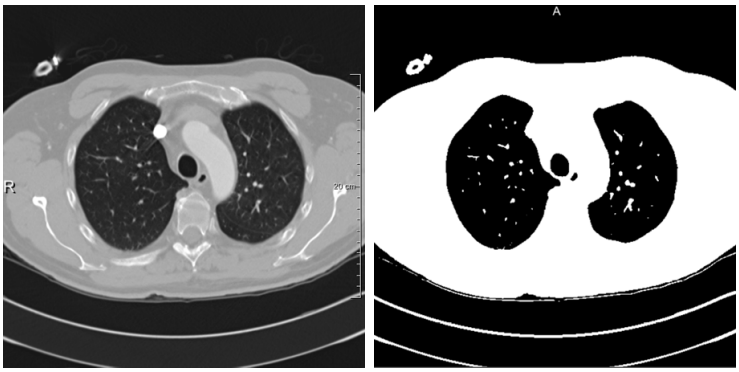

(a) (b)

Figure 15: (a) Original Image (b) Otsu threshold

3.3.2 Noise attenuation

As mentioned in the previous step although some non anatomical objects are removed with the threshold others still remain. In order to remove some of the non anatomical objects some noise reduction algorithms can be implemented[40, 24, 30, 13] because our method is based on the premise cited in the section 3.

Algorithms based on mathematical morphology, like an *opening*, will remove the desired objects if the right *SE* size is choose. Although this implementation presents some good results and better processing time there are some issues that can happen: edge deformation and loss of information's in air volumes inside a biological object (e.g. lungs).

Median filtering is a nonlinear filtering technique that has the characteristic of being edge preserving[11] and has been observed to be very effective for removing noise, especially impulse noise from one or two dimensional signals[10, 5]. Despite Bilateral filtering is presented as a noise attenuation and edge preserving filter intermediate results shows that median filtering has a better edge representation on binary images.

As the non biological objects can be spread along the Z plane (e.g. the bed) anisotropic filtering, like in X-Y plane, will achieve better smoothing results.

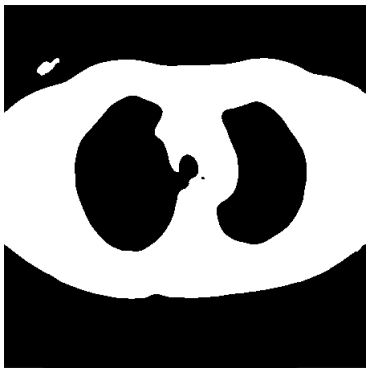

Figure 16: Median filtering of the previous segmented image.

3.3.3 Automatic Module

3.3.3.1 Air Detection As is possible that the previous step, noise attenuation, has removed some air volumes inside biological information that may contain crucial information it is necessary to recover this information back again. These air volumes have the characteristic of always being inside of the detected soft tissue. Good solutions pass to detect this inside non segmented volumes and modify volume value to the soft tissue value.

Region filling algorithm presented on section 2.2 is a good solution to fix this problem. Sollie's book Morphological Image Analysis[34] presents in chapter 6 also a good solution to the fill hole problem in binary images.

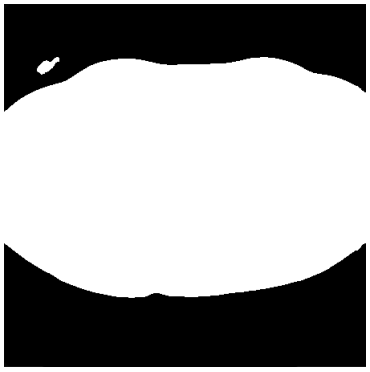

Figure 17: Region Filling filtering applied on the noise attenuation image.

3.3.3.2 With cropped images module Besides dealing with original data sets, the automatic implementation has the characteristic of being able to deal with user defined areas. User defined areas can be characterized by non original data sets modified by user(e.g. cropped volumes). If, in the corners of the image air volumes are represented, air detection algorithm will not perform his function because these extremes may not contain thresholded values that allows him to consider that area as a hole. In Figure 18 we present

a set of images that shows the possible combinations that can occur.

The automatic algorithm can detect this type of modified volumes performing a step of verification before the fill hole component. This verification is carried through an algorithm that checks for high intensities in corners combinations (like bottom and left, bottom and right...). This step verifies all the corner combinations and saves the identification of each corner combination that occurs to be processed in the next step: Border fill.

Border fill In order to get the air volumes in the segmentation this algorithm receives the corner combinations identifications and performs a pad with the thresholded value in each side of the corner combination (e.g. bottom and left). At this point we are able to apply the fill hole procedure in each corner combination. As this pad is effectuated only in combinations of two sides the fill hole will not include parts of the volume that need three sides of pad like we can verify in figure 18c. For each combination it is necessary to remove the padded information that was added after the fill hole filter.

Add combinations At this point there is a set of volumes (equal to the number of identified combinations) and it is necessary to convert them in one. For this a simple function is used that sums the various volumes and gives as output a single volume.

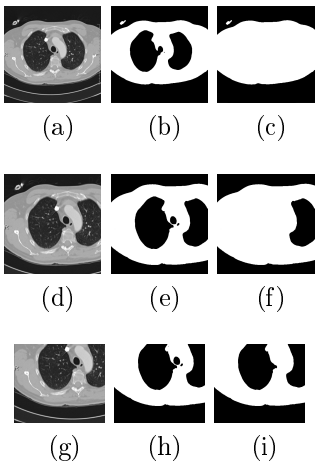

Figure 18: First row: a) Original image b) segmented image c) median image+fill hole; Second and third row cropped possibilities with the same logical sequence .

3.3.3.3 Minimum volume size filtering In figure 18b, that represents the original image filtered with a threshold followed by a median, it is easily identified the biological object and another smaller element situated on the top left of the image. Watching the original image it is perceptible that this is a non biological object that was not removed in the Noise attenuation component. These non biological components can have sizes which are not handled by the noise attenuation component because they can have random sizes.

Object identification or labeling is well documented in the literature[9, 32] therefore our solution is a 3D object labeling followed by a minimum size filtering of this objects. The biggest problem is how to determine these minimum size.

It is possible to define a percentage from knowledge obtained by analyzing all possible scans in the body, find the smallest possible components (like a scan of the fingers) and determine a default percentage. Another, better approach, is to get all the sizes of the objects on the data set and either get

the minimum size by performing a statistic method with Cluster analysis or construct a histogram of sizes and perform an automatic threshold method that calculates an output an threshold value like Otsu[29].

3.3.4 Semi-automatic Module

Although the automatic non biological removal was implemented assuming the premises, *"the image obtained from a scanner may contain non biological objects that have smaller area than the biological ones"*, can happen that for some rare cases (rares because is non logical to make a scan without focus on the biological part needed) that non biological objects can be bigger than the biological ones. Therefore a sub component was implemented which allows, with minimal user interaction, to choose what are the objects that we intend to remove.

First a minimum volume size filtering algorithm (as explained on section 3.3.3.3) is performed. After analyzing the 3D object labeling is presented a list of objects where the user decides which ones will be present on the final data set or no. After selecting the objects to keep on the data set is performed a algorithm that removes the unwanted objects.

3.3.5 Masking

After separating biological from non biological objects masking will combine the original image with the segmented one to retain only the desired information.

3.3.6 Volume reduction

Our implementation could be over on the previous step because the main goal was achieved but after verifying final outputs of several data sets it was observed that the volume contains information that was not needed (the removed areas) because the dimensions of the output of the masking step are

the same as the original volume.

The performance of 3D visualization methods like volume rendering is directly connected with the dimensions of the volume. This sub-component implements a intelligent cropping of the volume. This is done by finding the upper, bottom, left and right measures where biological information is present. Studies have shown that this reduction presents an average reduction on the data set of 41%[19].

3.4 Results

Several data sets were used with the object removal proposal and achieved the goal of the project. For execution time a data set with a dimension of $512 \times 512 \times 300$ was analyzed in an average machine equipped with an Intel Core 2 Duo E8400 @ 3.00GHz processor and 2.00 GB of RAM. The data set was applied to the different noise attenuation proposed and to the cropped images module. The proposed algorithm was implemented with ITK and the results of the table 1 are an average of five iterations.

			With cropped images module	
Number of slices	Opening	Median	Opening	Median
300	43,1802	49,8394	128,1342	138,3584

Table 1: Processing speed in seconds.

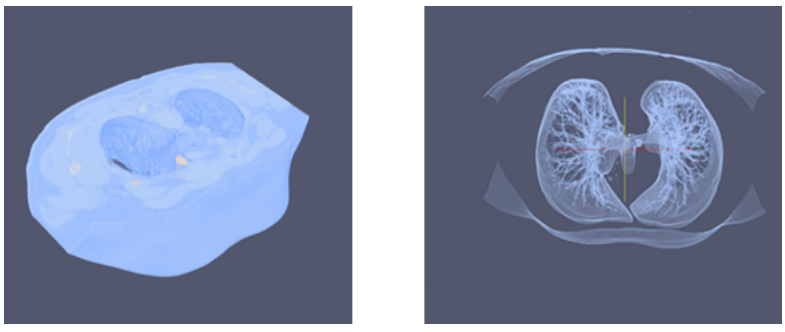

Figure 19: Final result of the implementation.

3.5 Conclusions

Air detection inside a biological object in an original data set is straight forward, but when there is user customization on the data set this can be a hard task. Although the proposed implementation to deal with this detection can handle with almost every possible cases there is one possibility that can be quite tricky to handle. If there is a data set that contains soft tissues from the left to the right (or for the top to the bottom) and then one of the parts has inside air volumes and the other does not, then the implementation to handle with user customized data sets will not produce the desired results.

For all other types of data sets the proposed implementation will remove the non biological objects and although text or logo information's, were not the goal of the project, will be removed as well. Because of this capacity of the implementation for removing noise in the data set future 3D visualizations can be much clearer without non biological objects occluding some parts to the user. Furthermore the use of object removal can be an important tool to save space in databases and results in important reductions in required rendering time.

4 Metal Artifact Reduction on Dental Areas

In modern dentistry, computer assisted procedures of mechanized dental implant are getting more attention day by day. Accurate knowledge of the 3D shape of teeth and the position of the roots is very important in many maxillo-facial surgical applications, endodontic procedures and treatment simulations.

In X-ray CT, Metal Artifact Reduction (MAR) has been a challenging problem. Many different approaches for MAR are found in the literature. The most obvious solution is to prevent metal artifacts by using less-attenuating materials (e.g. titanium) or devices with smaller cross-section. Haramati concluded that using higher energy x-ray beams gives no substantial artifact reduction[14].

The presence of metallic objects tends to generate strong artifacts in reconstructed CT images. The most important causes of metal artifacts are noise, beam hardening, the non-linear partial volume effect, and scatter. They can cause abrupt intensity changes especially in areas around the implant soft tissue pixels can now have smaller intensities or similar teeth intensity's. Therefore these soft tissues, that are easily removed with a simple threshold when metallic objects were not present, will be present in the final visualization as shown in figure 20.

4.1 Research Goal

Most often, these parts and organs must first be segmented slice by slice or even by defining regions with a tool to include or remove an area. Logically, this is a tedious and time consuming procedure. Many algorithms have been developed for the automatic segmentation of various tissues. In this regard, automatic segmentation of teeth, with metal implants, from the mandible and maxilla is a fairly new subject.

The aim of this component of the thesis is to create an automatic or

semi-automatic algorithm to perform an implementation that will allow a better 3D representation of the teeth and jaws area, increasing significantly their usability. Semi-automatic solution should require few interactions of the user(slice by slice approach would be unusable).

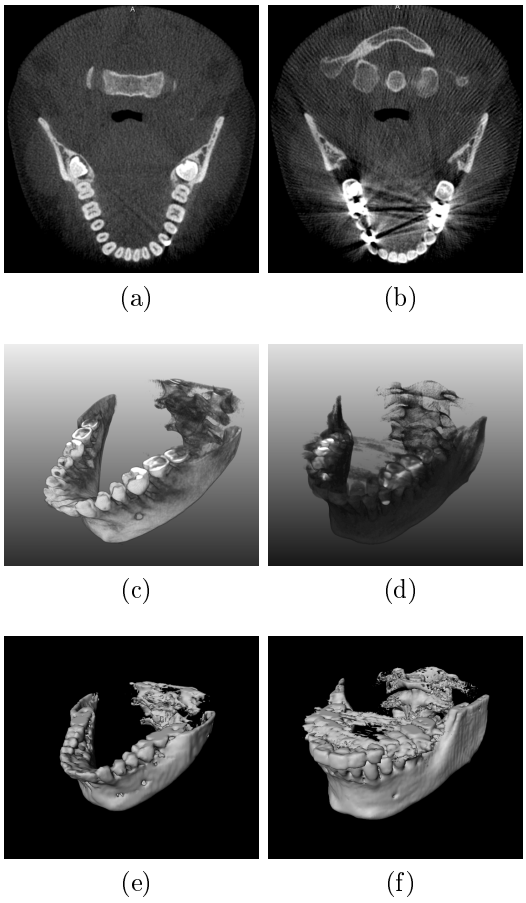

Figure 20: Overview representation: a) CT image without metal artifacts b) CT image with metal artifacts c) Volume Rendering view of a CT scan without metal artifacts d) Volume Rendering view of a CT scan with metal artifacts e) Surface Rendering view of a CT scan without metal artifacts f) Surface Rendering view of a CT scan with metal artifacts

4.2 Input Data Characteristics

CT examination consists of a series of plane cross section slices. Typical slices number in series is between 50 and 200. Typical slice matrix size is 512*512. Slice thickness may be $0.5mm$, $1mm$ or bigger (depending on the case). Pixel size in slice plane is usually $0.25mm$ or $0.5mm$.

Jaw bone has a boundary layer from cortical bone (compact), which has *Roentgen*[2] density in range 1200∽1800 *HU*. Inside of bones there is spongy bone, which has roentgen density in range 200∽1200 *HU* [20].

Teeth consist of two main tissues: enamel and dentine (figure 21). Enamel is hardest tissue in human body and has *Roentgen* density in range 2100∽4000 *HU*. Dentin is closer to cortical bone and has *Roentgen* density in range 1400∽2000 *HU* (as seen in figure 21a). Jaw bone density values are between 1200 and 4000 *HU*. Metallic implants CT numbers are in the range of 8000 up to 50000 *HU* [39].

As said previously, upper limit on modern medical scanners is approximately 4000 *HU*, therefore the presence of metallic implants will cause clipping of the reconstructed image. If low frequency artifacts near the metal have high amplitudes, the result can be a complete blurring and distortion of the true contours of a metal implant [39].

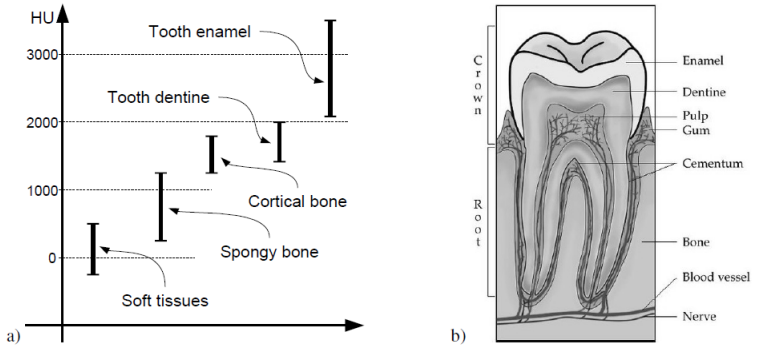

Figure 21: a) Typical ranges in Hounsfield units b) Tooth scheme

[2]Röntgen or Roentgen it is a unit of measurement for exposure to ionizing radiation (such as X-ray and gamma rays).

4.3 State of the Art

Several techniques have been proposed for MAR. These methods can be categorized in two main classes, namely sinogram-based and image-based methods[2].

4.3.1 Sinogram-Based Methods

Various metal artifact reduction algorithms have been suggested in the literature [41]. The general hypothesis lying behind the development of metal artifact reduction algorithms is that the artifacts are caused by deviations of the acquisition model assumed by the reconstruction from the true acquisition process, consequently, improving the acquisition model should reduce artifacts.

Most of the currently available sinogram based MAR algorithms are based on correction of raw data sinograms[1]. They consist on modifying the reconstruction algorithms, that don't handle with the MAR problematic, in which metal objects are usually considered opaque and data corresponding to projection lines through metal objects are defined as missing data. They can be divided into two groups [7]:

- **Projection completion methods**: missing or corrupted area is replaced by data obtained by interpolations [12, 17], pattern recognition [25] or linear prediction methods.
- **Iterative methods**: missing data in the iterative methods [31, 38] is ignored.

Linear interpolation of the missing data is one popular technique[17]. Metallic objects are detected by a simple threshold because as previously mentioned there is a considerable difference between them and other tissues. The extracted image is forward projected to determine the projections in the sinogram space which are affected by metallic objects. These projections

are then replaced by linear interpolation of other projections in the same projection angle. Finally, the corrected image is obtained from the reconstruction of the corrected sinogram through application of the inverse *Radon* transform.

4.3.2 Image-Based Methods

The second group of MAR methods operates in image rather than in sinogram space. In these approaches, artifacts are treated as unwanted objects to be removed using enhancement methods. Obviously, the degree of enhancement is limited to the adequation of the applied algorithm. A precise detection of regions affected by metallic artifacts is a complicated task owing to the intrinsic ambiguities between CT numbers of artifacts and surrounding tissues.

4.3.2.1 Virtual Sinograms Methods

Virtual sinograms methods [2] uses the concept of virtual sinograms produced by forward projection[3] of CT images in DICOM format for MAR. Customization parameters used in this procedure are similar to those of the scanner. In this method, the projection data affected by metallic objects are first detected in the sinogram space through segmentation of metallic implants in the CT image followed by forward projection of the metal-only image. Thereafter, the extracted sinogram bins are replaced by interpolated values of adjacent bins using the spline interpolation technique. The corrected sinogram is then reconstructed to generate an artifact-free CT image. The reconstruction algorithm used is based on a filtered back projection which utilizes the inverse *Radon* transform where the elements of the sinogram matrix are backward projected to the image matrix.

[3]Forward Projection is performed using a MATLAB (The MathWorks Inc., Natick, Massachusetts, USA) routine, which generates fan beam projection data from input images according to a predefined acquisition geometry.

4.3.2.2 Segmentation of Teeth in CT Volumetric Dataset by Panoramic Projection and Variational Level Set

Hosntalab et al. [15] have proposed a teeth segmentation with jaws separation and metal artifact reduction procedure. First the head mask is extracted from the background by an *Otsu* thresholding [29](figure 22b) and then bony tissues are separated from non-bony tissues by applying a level set technique [8, 23, 28](figure 22c). The Hamilton-Jacobi equation is written as:

$$\frac{\delta\phi}{\delta t} = C(x)(\varkappa + V_0)|\nabla\phi| + \nabla C.\nabla\phi + \frac{V_0}{2}x.\nabla C|\nabla\phi|, \tag{11}$$

where ϕ is the level set distance function; $\varkappa$ is the curvature and controls the minimum length and continuity of the contour; V_0 is a constant force that imposes to the contour; and is defined based on the blurred version of the original image as follows:

$$C(x) = \frac{\alpha}{1 + \nabla[G_\sigma(x) * I(x)]}, \tag{12}$$

where *I (x)* and $G_\sigma = \sigma^{-\frac{1}{2}}e^{-|x^2+y^2|}/4\sigma$ are the original image and the Gaussian function, respectively. The second term in (11) acts as a stopping function, and the last term is employed to minimize the contour area during the level set evolution. Equation (11) was employed to segment bony tissues from other tissues in CT data-sets.

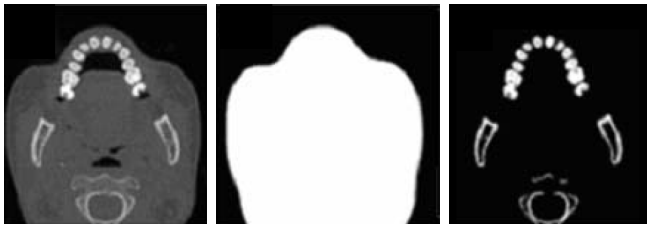

(a) (b) (c)

Figure 22: a) Original CT slice; b) Otsu thresholding from the original CT slice; c) Level set technique

Afterwards upper and lower jaw are separated by finding the slice that does not include teeth to make a panoramic re-sampling of the data-set. This re-sampling is used to implement teeth segmentation by a variable level set[42]. Some customizations were done but as this subject of teeth separation goes out of the thesis it will not be described here.

After, a metal artifact reduction step is performed by finding the slices where metal implants exist and applying a Butterworth low pass filter i.e:

$$H(u,v) = \frac{1}{1 + [D(u,v)/D_0]^{2n}} \tag{13}$$

Where the order of the filter (n) and cutoff frequency distance (D_0) are selected as 5 and 2%, respectively.

Small elements were still present and for that was generated a binary mask and applied a size filter removal. As artifacts lines were still remaining it was employed morphological erosion followed by opening on gray CT images to reduce them.

4.3.2.3 Rapid Automatic Segmentation and Visualization of Teeth in CT-Scan Data

In this study [3] techniques for separation of mandible and maxilla, segmentation of teeth and metal artifact reduction are proposed. There are 4 main steps: separation of mandible and maxilla, dental region separation, teeth segmentation and metal artifact reduction.

A pre-processing step, to remove salt and pepper noise from the CT images, is done. Originally a 3D median filter was used but as the processing times were not satisfactory this filter was changed to a 2D mean filter that was faster than the median without significantly affecting the final results.

Mandible and maxilla separation is based on Maximum Intensity Projection (MIP) and a region separation algorithm. First a MIP of the data-set in the Y direction is obtained. As this projection data-set has non bone tissues it is applied a threshold filter to remove them. In each slice, is calculated the

distance of the left edge of the image to the nearest bone pixel in that row. A line is drawn from the left side of the image to the first bone pixel in the slice in which the mentioned distance is a maximum compared to the others slices. From this pixel, a vertical line is drawn up till the first bone pixel is reached. On this vertical line, the previous procedure is performed until moving right or upwards is not possible, figure 23a). The distance between the first and last horizontal line is calculated and all pixels beneath the step like line are shifted downwards the amount of this distance in the volumetric data. The resulting gap is then filled with black pixels as represented in figure 23b). This volume is then separated into two volumes with one containing the mandible and another containing the maxilla.

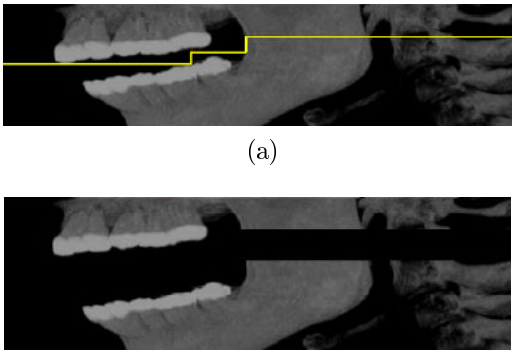

(a)

(b)

Figure 23: (a) Separation process (b) Separated jaws

Dental region separation is performed to achieve higher processing speeds. To separate the dental region the MIP of each jaw in the z direction was obtained. A threshold filter is then used to remove all pixels with values lower than the enamel and finally a bounding rectangle of the mask of the teeth is used to crop all the images in the data-set reducing the processing time.

The segmentation process is basically a region growing procedure performed in 3 steps involving 4 thresholds:

1. **Threshold 1 (TH1)**: the aim is to select the seed points to perform region growing. The threshold value used is based on the enamel of the teeth. In cases which metal artifacts are present they will also be chosen as seed points because they have higher intensity's.

2. **TH**2: this is the most important threshold. The initial value of this threshold is selected slightly above the pixel value of bones which the roots of the teeth reside in. This is a variable threshold which stops the teeth region from spreading into the bones.

3. **TH**3: In the beginning of the algorithm a mean filter was used for smoothing and noise reduction in all images. The result of this filter caused a reduction in the value of pixels which are located in boundary locations in which their neighbors have lower values than themselves. If these pixels are part of the teeth they would not be included as teeth because of their decreased value. The value of this threshold was found by studying the pixel values of the teeth in boundary locations after the mean filter.

4. **TH4**: this threshold is chosen so that all pixels above it are bony tissue and all pixels below it are non-bony tissue. This threshold is used to achieve higher processing speed and to remove all none bone tissue.

The following condition exists between the thresholds: $TH1 > TH2 > TH3 > TH4$.

As said before there are three segmentation steps:

- **Step 1**: the first step performs a region growing algorithm. All pixels higher than TH1 are marked as the seed points.

- **Step** 2: the pixels that are included in this step fulfill the following conditions: (a) their value is higher than TH4 (i.e., they are bony tissue) and (b) they have an already segmented neighbor in the neighborhood of 1 in all directions whose value is above TH2.

- **Step 3**: boundary regions degraded due to the mean filter are added to the teeth region.

Metal artifact reduction is used in places where the metal artifacts have introduced false positive pixels. A weighted image of the segmented teeth in the Z direction is constructed. A weighted image is an image in which the value of each pixel is equal to the total number of slices in which the corresponding pixel is segmented as being part of the teeth. Passing this mask through a multiple threshold filter a secondary mask is acquired which does not have pixels corresponding to artifacts in it. As the threshold filter has also removed some of the pixels which might correspond to the teeth a dilate filter was performed in the selected mask to compensate the pixels that might have been removed.

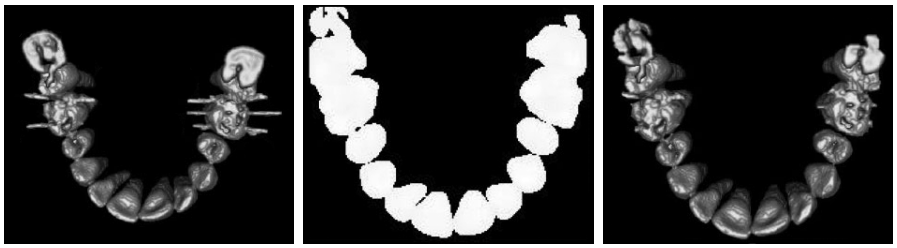

(a) (b) (c)

Figure 24: Metal artifact Reduction: a) Original representation b) Mask example c) Final representation

4.3.2.4 A New Approach in Metal Artifact Reduction for CT 3D Reconstruction

Naranjo et al. [37] has show a new point of view in MAR methods proposing a new approach based on mathematical morphology(ASF filtering) in the polar domain. The paper suggested a conversion on each slice from the Cartesian to the polar domain for the correction of the streaking artifacts.

As previously mentioned mathematical morphology algorithms for artifact or noise reduction depends on the correct choice of the SE shape, size and

orientation. Naranjo has observed that in order to remove streaking artifacts the optimum SE would be the combination of different SE perpendicularly oriented to each ray. The solution was to transform the image into a new domain for all the streaking lines have the same orientation with the aim of using a single SE for the whole image.

Algorithm 1 shows the process followed in order to reduce image artifacts.

Algorithm 1 MAR algorithm by Naranjo et al.

1. cavities mask definition$\Rightarrow I_{msk}$
2. streaking origin detection
3. Cartesian domain $\Rightarrow$ polar domain
4. alternate sequential filtering $\Rightarrow I_{original}$
5. polar domain $\Rightarrow$ Cartesian domain
6. combination

First, the original image was segmented using hard threshold in order to detect the cavities ($I_{original} < T$) which were dependent on the density values of the different structures in CT study. As a result of this process a mask (I_{msk}) was defined with the cavities set to 1 and the remaining pixels set to 0. This way, cavities were preserved from the effects of the ASF since they don't present problems due to artifacts, and are successfully reconstructed. After this, the equation of the streaking rays were extracted by granulometry processing, and then, the streaking origin was automatically detected as the solution of the resulting overdetermined system. Later, the original image was converted from Cartesian into polar domain being the streaking origin, the central point (x_c, y_c) as in figure 25.

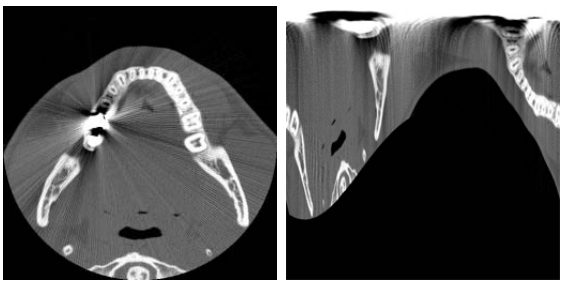

(a) (b)

Figure 25: (a) Original CT image in Cartesian coordinates (b) CT image converted to polar coordinates.

The image was then filtered with the alternate sequential filter described on 2.2 and reconverted into the Cartesian domain with the same focus. At last, the final image was obtained merging the original image and the filtered one in the following way:

$$I_{final} = I_{original} \times I_{msk} + I_{filtered} \times (1 - I_{msk}) \tag{14}$$

Consequently, those image areas with density structures higher than a threshold (not cavities) were filtered and smoothed.

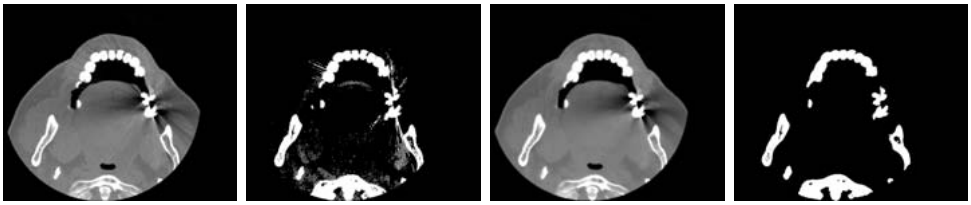

(a) (b) (c) (d)

Figure 26: (a) Original images (b) Original images thresholded (c) Processed images (d) Processed images thresholded.

4.3.3 Conclusions

Although sinogram-based methods are accurate, they require manipulation of raw projection data. Unfortunately these types of approaches are impossible to be analyzed in our case since it assumes access to the decoded projection data that is dependent on the scanner's brand or even model.

Image-Based Methods present a more practical solution to the MAR problem. Virtual Sinograms methods present interesting results but they still need some previous knowledge (geometry and projection parameters) from the scanner device, making them dependent from some parameters to design a robust solution. The proposed artifact reduction algorithm, should avoid these difficulties by working directly in the CT images with image processing filtering. Hosntalab et al.[15] level set method for segmentation of teeth and jaws has an accurate representation but the need to perform numerous mathematical procedures makes it to be not considered a fast method [3]. The artifact reduction implemented is based in a low pass filter with a morphological procedure to reduce small noise components that were remaining. Although the erosion filter reduces the noise components it can lead to some loss in the teeth representation. In the Akhoondali et al. [3] study, a new method for mandible and maxilla separation is presented. The method works with the restriction that patient mouth must be open when the CT scanning is performed. The artifact reduction method works locally (only in slices that contain false positive pixels) but does not define regions to perform the method (some teeth that can be well represented and without metal artifacts are submitted to the reduction algorithm as well). Although some teeth information may be excluded in the weighted algorithm it leads to a good detection of the artifacts lines, which are easily removed with a threshold filter.

Naranjo method represents the turning point on the MAR algorithms. The utilization of a new system coordinates (polar coordinates) with mathematical morphology to reduce artifacts has lead to an image improvement

and consequently to a reduction of streaking artifacts. Beam hardening surrounding metallic objects are not completely removed because the use of a bigger SE could erase some unwanted information. Another issue is that the current implementation only considers a single metallic object. Streaking origin detection is also possible improvement.

4.4 Method

From the previous reviewed methods Naranjo approach presents solid theoretical and practicals results. Aspects as the use of a bigger SE and the use of multiple objects can be improved so the proposed method is based on it. In this section we present an extension of the metal artifact reduction method in a specific structure of the human body: jaws. This part of the body was selected because it is the structure where these kind of anomalies are presented more often.

As identified before, one major limitation on the algorithm is the size of the SE. Beam hardening surrounding the metallic objects are not completely removed because the use of a bigger SE could erase some unwanted information (teeth and jaw) so filtering only the regions where the scattering effect (near the metal implant) is bigger would allow the use of a bigger SE. Polar coordinate system defines each point by its radial and angular coordinates therefore defining a maximum radial distance would allow a region filtering of the image to apply a bigger SE. Our method proposes to work locally, defining regions that are on the neighborhood of the metallic implant with a maximum radial distance (p_{max}) on the polar image and protecting neighborhood teeth with a enamel projection image.

Algorithm 2 Region MAR algorithm

1. Masks (Cavities Mask + Enamel Mask)
2. Streaking origin detection
3. For(each streaking origin)
   (a) Cartesian domain ⇒ Region polar domain (Cavities Mask + Enamel Mask) .
   (b) Labeling the region enamel mask.
   (c) Mathematical morphology filtering of the region cavities mask.
   (d) Polar domain ⇒ Cartesian domain
   (e) Mean

4.4.1 Masks

Cavities Mask

The aim of this step is to create a segmented volume that represents the jaw and teeth structures. As analyzed in 4.2 a tooth (dentine and enamel) has a *Roentgen* density in range 1400∽4000 *HU* and the jaw structure has a density in range 1200∽1800 *HU*, therefore a threshold value lower than 1200 *HU* will contain both structures. This segmentation will contain more structures behind the desired, teeth and jaw, so a connected components filter(on the z axis) is applied in order to label the objects present and finally filter the biggest one in area.

Enamel Mask

Enamel mask has the aim to create a protection from the neighborhood teeth of a streaking origin, in a process that will be detailed in later steps. This mask consists in a enamel threshold projection and gives a good representation of the position of each tooth without beam hardening and the streaking

effects caused by the presence of the metallic objects because, as seen before, enamel has the characteristic of being the tissue with the biggest intensity value on the body (*Hounsfield* values in the range of 2100∽4000 *HU*). As this mask has a crucial role in the algorithm the threshold value can be adjusted interactively. Figure 27 shows enamel projections with threshold values around the enamel *Hounsfield* value.

(a) (b) (c)

Figure 27: (a) Wrong enamel threshold projection (b) Projection with metal artifacts noise (c) Good enamel projection

4.4.2 Streaking Origin Detection

Metallic implants have an intensity that none of the tissues of our body can have therefore a simple threshold operation with a lower value of 8000 *HU* will detect these artifacts. Each seed point is calculated by finding the center coordinate between the left, right, up and down extremities for each object.

4.4.3 Cartesian to Polar Domain

For each metallic object detected in the previous step an image is created which represents a region of the original one in the polar domain. The image

is converted with equations 9 and 10. As said before the size of the radius p_{max} defines the size of this region, so the polar image will contain only pixels lower than p_{max}. Figure 28a shows in red the size of the radius that will be selected to do the region filtering in the polar domain as seen in image 28b .

From the enamel mask is also created an region polar domain image that as the same center point and radius as seen on figure 28c.

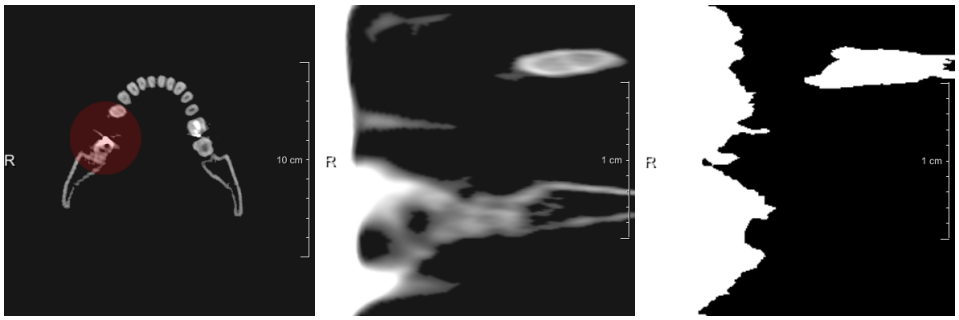

(a) (b) (c)

Figure 28: (a) Cavities mask and size of the radius in red (b) Region polar domain image created from cavities mask image (c) Region polar domain image created from the enamel threshold projection image.

4.4.4 Labeling the region enamel mask

The aim of this step is to identify other teeth that can be present in the region in order to "protect" them from the morphological filtering that will be done. This labeling is done by the Connected Components algorithm described on section 2.2.

4.4.5 Mathematical Morphology on region cavities mask

After, one of the mathematical filter with artifact reduction characteristics described before on section 2.2 is used on the region cavities mask. As show in image 28b, streaking rays are along the horizontal axis, therefore the SE will have only an vertical orientation.

4.4.6 Polar domain to Cartesian domain

Once the artifact reduction filter based on mathematical morphology is processed, the polar image pixels are replaced on the same region of the cavities mask. The enamel mask is used to "protect" neighborhood teeth of a streaking origin. Before replacing a pixel on the cavities mask (from the filtered with mathematical morphology) it is verified if in the enamel polar image the correspondent pixel is identified as being the tooth of the streaking origin or another one. If is the tooth of the streaking origin the pixel is replaced by the pixel of the image filtered with mathematical morphology. If not, the current pixel is not replaced. This is the masking operation that allows to use a bigger SE sizes on the previous step.

4.4.7 Mean

To deal with the multiple streaking origins after the previous conversion a mean operation between the current streaking origin result and the previous is done. If there is only one streaking origin in the image this step is ignored.

4.5 Results

Results with the several mathematical morphology operations proposed on section 2.2 are presented. The dataset used is from a lower jaw scan and is highly affected by the metal implants (29).

(a) (b) (c)

Figure 29: (a) Original CT image (b) Thresholded image (c) 3D reconstruction

All the filters were tested with the same size of radius and SE. The tested mathematical morphology operations were:

1. Opening ⇒ Closing
2. Closing ⇒ Opening
3. Mean(Closing, Opening)
4. Alternated Sequential Filtering

Only an opening operation is performed first than an closing because it can lead to loss of information on the object.

Figures 30,31,32,33 shows the different mathematical morphology operations (ordered) applied to different images in order to be possible to analyze the filters. For all the figures, in the (c) column, is possible to observe the region where the mathematical filter is applied because they present smoothed areas caused by the filtering. From the results on the (d) column is observed that Closing ⇒ Opening and Mean(Closing, Opening) present very similars results because the logic operation sequence is the same. It is curious to notice that the ASF results are not so good as the one presented by Opening

$\Rightarrow$ Closing and Closing $\Rightarrow$ Opening. From the first image on the column (d) it is possible to observe that Closing followed by a Opening operation present better results.

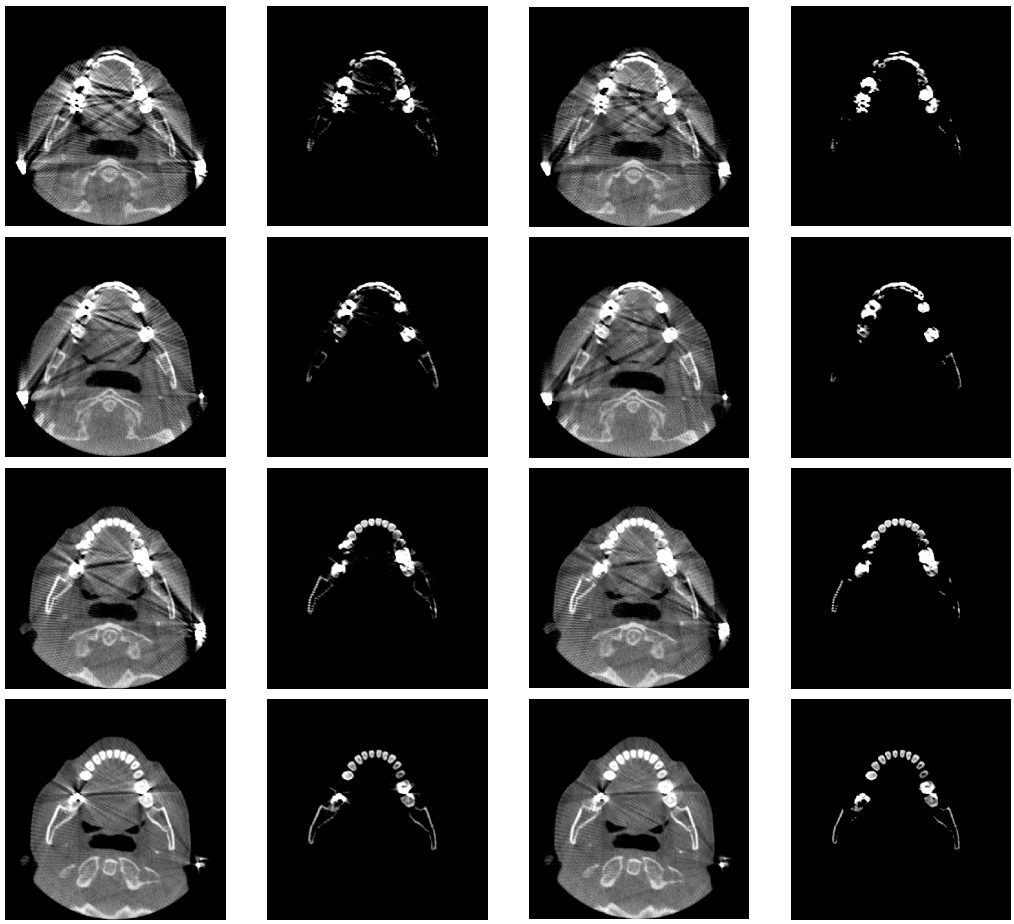

(a) (b) (c) (d)

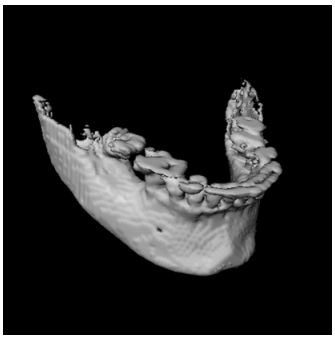

(e)

Figure 30: (a) Original image (b) Cavities mask (c) Opening ⇒ Closing applied to the original image (d) Opening ⇒ Closing applied to the cavities mask (e) Surface Rendering from the filtered dataset

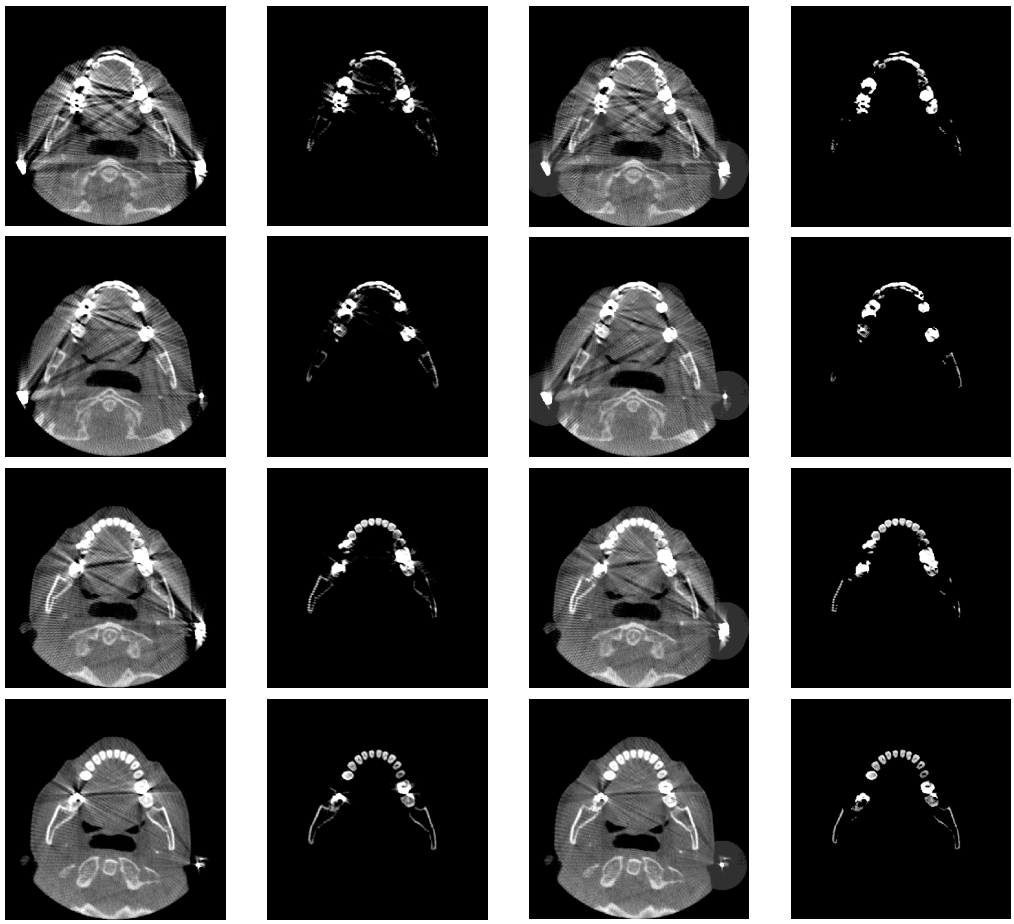

(a) (b) (c) (d)

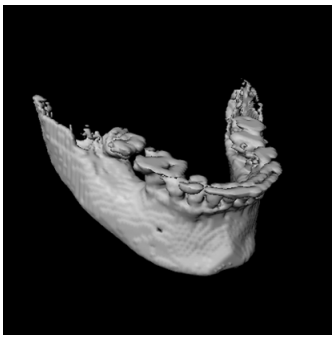

(e)

Figure 31: (a) Original image (b) Cavities mask (c) Closing ⇒Opening applied to the original image (d) Closing ⇒Opening applied to the cavities mask (e) Surface Rendering from the filtered dataset

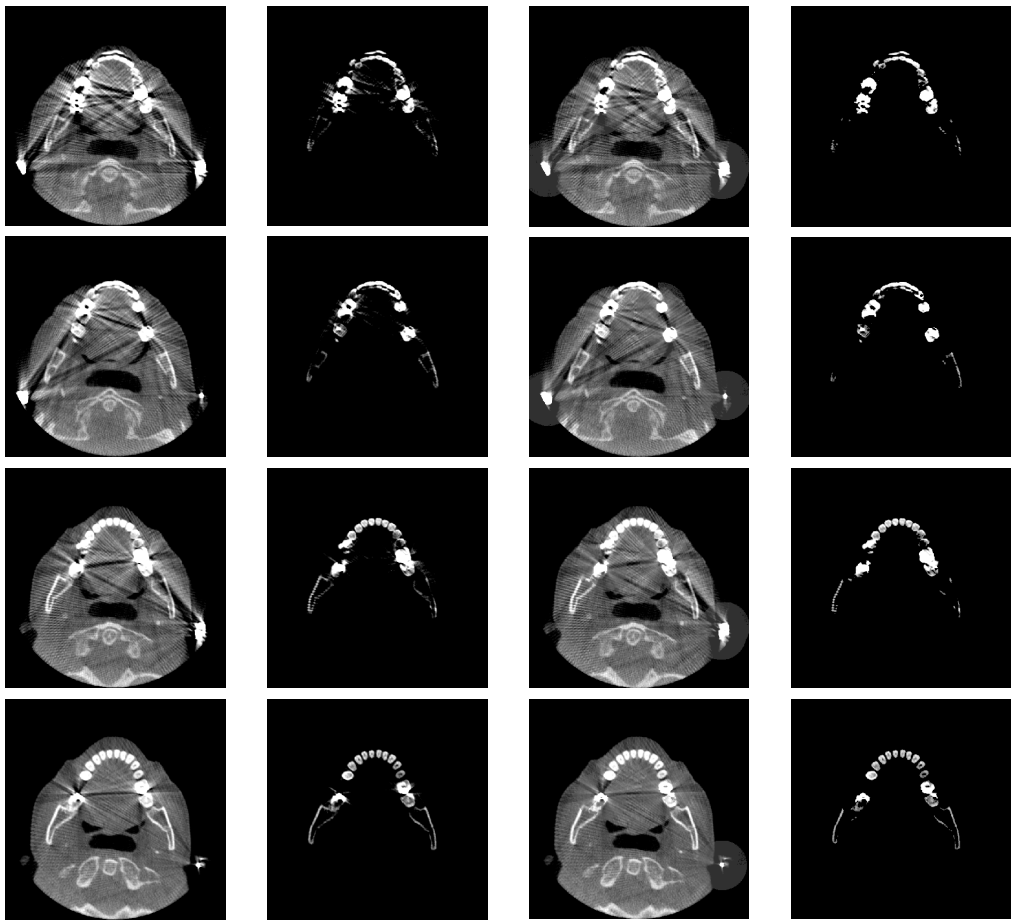

(a) (b) (c) (d)

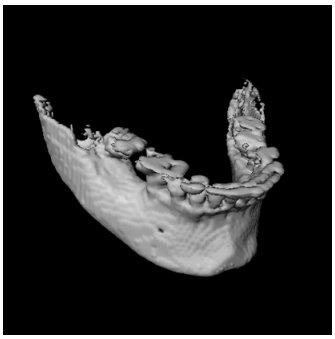

(e)

Figure 32: (a) Original image (b) Cavities mask (c) Closing ⇒Opening applied to the original image (d) Closing ⇒Opening applied to the cavities mask (e) Surface Rendering from the filtered dataset

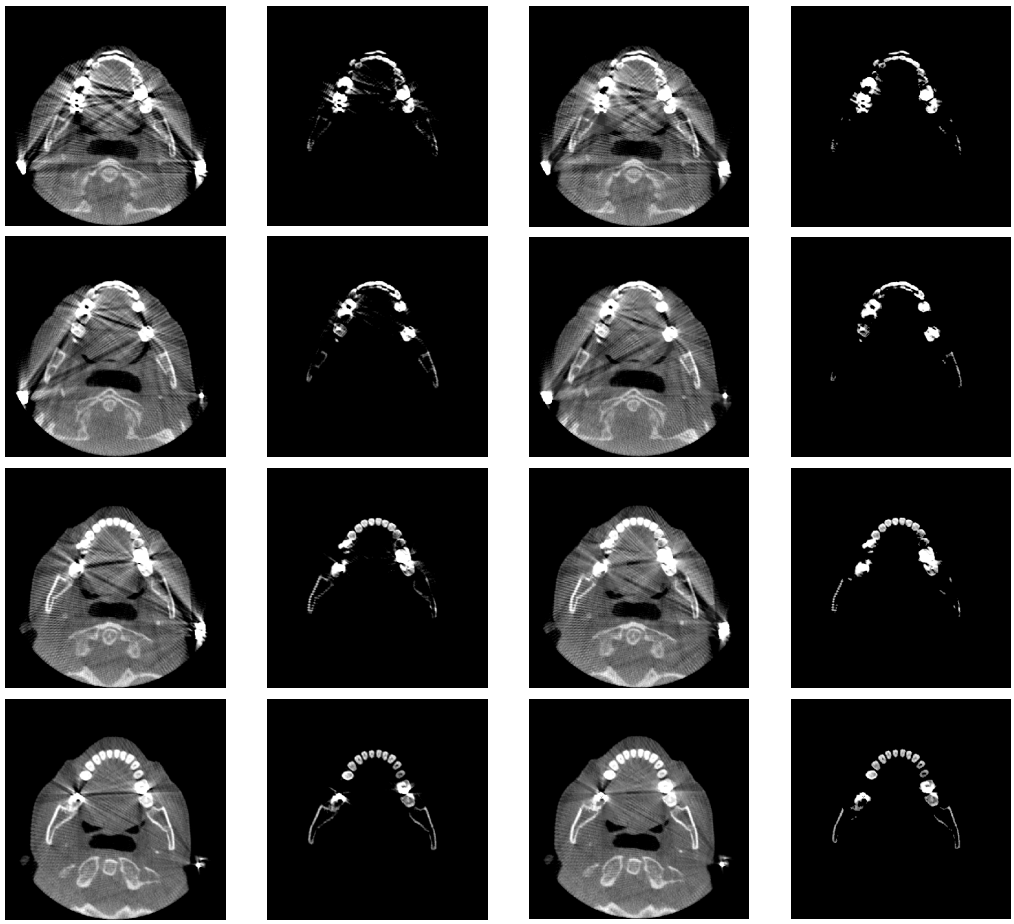

(a) (b) (c) (d)

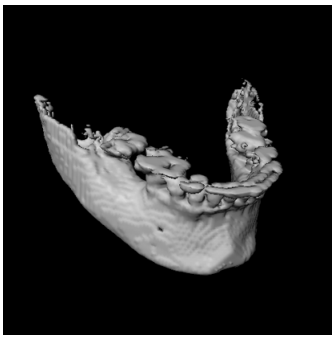

(e)

Figure 33: (a) Original image (b) Cavities mask (c) ASF applied to the original image (d) ASF applied to the cavities mask (e) Surface Rendering from the filtered dataset

4.6 Conclusion

The approach described in this paper presents an extension to the Naranjo work which represents a new point of view in MAR methods since it uses only information provided by the DICOM files. A set of techniques for dealing with some limitations of the Naranjo approach for Metal Artifact Reduction was presented.

The presented method suggests to work the image locally, inside a ray distance, with the aim of reducing the area for applying the mathematical morphology filter in the polar domain of this region. The enamel mask concept is included to identify undesired objects (teeth) that this region may still contain allowing the use of a bigger size of the SE element.

A threshold based method is presented to identify each streaking origin. This threshold is performed together with the information of the *Hounsfield* characterization of the metal. A mean operation between the current streaking origin result and the previous is suggested to deal with the problematic of the multiple streaking origin.

The results achieved are so far satisfactory regarding both the final image and surface rendering. Future work should focus on a method for automatic detection of the enamel mask, improvement of the streaking rays origin by detecting big discrepancy values between neighborhood pixels, other mathematical formulations to handle with multiple metallic objects and the testing of new mathematical morphology filters.

5 Final Conclusion

In this thesis two distinct problems in the area of medical image processing were abborded. Although the subjects were different, both intend to obtain better visual representation.

The first, "Non Anatomical Object Removal from CT Images", deals with problematics like oclusions provoked by undesired objects, hospital logo or text that can be engraved in the image. Two solutions were presented: automatic and semi-automatic. The automatic solution achieves good results but may present some issues with modified data sets. Semi-automatic is an alternative method that gives a solution to possible issues that can occur with the automatic one. The ability to handle the different variations in the CT images shows the robustness of the algorithm.

The second subject, "Metal Artifact Reduction on Dental Areas", deals with the artifacts added in the image caused by metal implants and is based on the Naranjo work. A set of new techniques and concepts is presented that improves the previous algorithm. Despite the fact that it is not possible to affirm with accuracy that the teeth are precisely represented the results have shown that a significant improvement is achieved even in highly affected images.

References

[1] M. Abdoli, MR Ay, A. Ahmadian, N. Sahba, and H. Zaidi. A novel approach for reducing dental filling artifact in CT-based attenuation correction of PET data. Springer.

[2] M. Abdoli, M.R. Ay, A. Ahmadian, and H. Zaidi. A virtual sinogram method to reduce dental metallic implant artefacts in computed tomography-based attenuation correction for PET. *Nuclear Medicine Communications*, 2009.

[3] H. Akhoondali, RA Zoroofi, and G. Shirani. Rapid Automatic Segmentation and Visualization of Teeth in CT-Scan Data. *Journal of Applied Sciences*, 9.

[4] J.F. Barrett and N. Keat. Artifacts in CT: Recognition and Avoidance1. *Radiographics*, 24(6):1679, 2004.

[5] A.C. Bovik, T.S. Huang, and D.C. Munson. The effect of median filtering on edge estimation and detection. *IEEE Transactions on Pattern Analysis and Machine Intelligence*, pages 181–194, 1987.

[6] R. Brunelli. *Template Matching Techniques in Computer Vision: Theory and Practice*. Wiley-Blackwell, 2009.

[7] DE Bruno. Iterative Reconstruction for Reduction of Metal Artifacts in Computed Tomography.

[8] V. Caselles, R. Kimmel, and G. Sapiro. Geodesic active contours. *International journal of computer vision*, 22(1):61–79, 1997.

[9] Michael B. Dillencourt, Hannan Samet, and Markku Tamminen. A general approach to connected-component labeling for arbitrary image representations. *J. ACM*, 39(2):253–280, 1992.

[10] J. M. Fitzpatrick and M. Sonka. *"Handbook of Medical Imaging, Volume 2. Medical Image Processing and Analysis (SPIE Press Monograph Vol. PM80)"*. SPIE–The International Society for Optical Engineering, 1 edition, June 2000.

[11] N. Gallagher Jr and G. Wise. A theoretical analysis of the properties of median filters. *IEEE Transactions on Acoustics, Speech and Signal Processing*, 29(6):1136–1141, 1981.

[12] G.H. Glover and N.J. Pelc. An algorithm for the reduction of metal clip artifacts in CT reconstructions. *Medical Physics*, 8:799, 1981.

[13] Rafael C. Gonzalez and Richard E. Woods. *Digital Image Processing (3rd Edition)*. Prentice-Hall, Inc., Upper Saddle River, NJ, USA, 2006.

[14] N. Haramati, RB Staron, K. Mazel-Sperling, K. Freeman, EL Nickoloff, C. Barax, and F. Feldman. CT scans through metal scanning technique versus hardware composition. *Computerized medical imaging and graphics: the official journal of the Computerized Medical Imaging Society*, 18(6):429.

[15] M. Hosntalab, R. Aghaeizadeh Zoroofi, A. Abbaspour Tehrani-Fard, and G. Shirani. Segmentation of teeth in CT volumetric dataset by panoramic projection and variational level set. *International Journal of Computer Assisted Radiology and Surgery*, 3(3):257–265, 2008.

[16] GN Hounsfield. Computerized transverse axial scanning (tomography): Part 1. Description of system. *British Journal of Radiology*, 46(552):1016, 1973.

[17] WA Kalender, R. Hebel, and J. Ebersberger. Reduction of CT artifacts caused by metallic implants. *Radiology*, 164(2):576, 1987.

[18] J. Kim, Y. Hu, C. Chan, S. Eberl, W. Cai, D. Feng, and M. Fulham. Maximum intensity projection (MIP) visualization and navigation of

fused PET/CT with automated bed/linen removal. In *Society of Nuclear Medicine Annual Meeting Abstracts*. Soc Nuclear Med, 2007.

[19] Jinman Kim, Youmo Hu, Stefan Eberl, David Feng, and Michael Fulham. A fully automatic bed/linen segmentation for fused PET/CT MIP rendering. *J NUCL MED MEETING ABSTRACTS*, 49, 2008.

[20] P. Krsek, M. Spanel, P. Krupa, I. Marek, and P. Cernochov. Teeth And Jaw 3D Reconstrucion In Stomatology. In *Medical Information Visualisation-BioMedical Visualisation, 2007. MediVis 2007. International Conference on*, pages 23–28, 2007.

[21] M. Levoy. Display of surfaces from volume data. *IEEE Computer graphics and Applications*, 8(3):29–37, 1988.

[22] W.E. Lorensen and H.E. Cline. Marching cubes: A high resolution 3D surface construction algorithm. In *Proceedings of the 14th annual conference on Computer graphics and interactive techniques*, page 169. ACM, 1987.

[23] R. Malladi, JA Sethian, and BC Vemuri. Shape modeling with front propagation: A level set approach. *IEEE Transactions on Pattern Analysis and Machine Intelligence*, 17(2):158–175, 1995.

[24] P. Maragos and R. Schafer. Morphological skeleton representation and coding of binary images. *IEEE Transactions on Acoustics Speech and Signal Processing*, 34(5):1228–1244, 1986.

[25] RL Morin and DE Raeside. A pattern recognition method for the removal of streaking artifact in computed tomography. *Radiology*, 141(1):229, 1981.

[26] H. Müller, J. Heuberger, A. Depeursinge, and A. Geissbühler. Automated Object Extraction for Medical Image Retrieval Using the Insight Toolkit (ITK). *Information Retrieval Technology*, pages 476–488.

[27] H. Müller, J. Heuberger, and A. Geissbuhler. Logo and text removal for medical image retrieval. In *German Workshop on Medical Image Retrieval (BVM), Springer Informatik Aktuell, Heidelberg*. Springer, 2005.

[28] S. Osher and J.A. Sethian. Fronts propagating with curvature-dependent speed: algorithms based on Hamilton-Jacobi formulations. *Journal of computational physics*, 79(1):12–49, 1988.

[29] N. Otsu. A threshold selection method from gray-level histograms. *IEEE Transactions on Systems, Man and Cybernetics*, 9(1):62–66, January 1979.

[30] S. Paris, P. Kornprobst, J.T. Tumblin, and F. Durand. Bilateral Filtering: Theory and Applications. *Foundations and Trends® in Computer Graphics and Vision*, 4(1):1–75, 2008.

[31] D.D. Robertson, J. Yuan, G. Wang, and M.W. Vannier. Total hip prosthesis metal-artifact suppression using iterative deblurring reconstruction. *Journal of computer assisted tomography*, 21(2):293, 1997.

[32] H. Samet and M. Tamminen. Efficient Component Labeling of Images of Arbitrary Dimension Represented by Linear Bintrees. *IEEE TRANSACTIONS ON PATTERN ANALYSIS AND MACHINE INTELLIGENCE*, pages 579–586, 1988.

[33] J. Serra and L. Vincent. An overview of morphological filtering. *Circuits, Systems, and Signal Processing*, 11(1):47–108, 1992.

[34] P. Soille. *Morphological image analysis: principles and applications*. Springer-Verlag New York, Inc. Secaucus, NJ, USA, 2003.

[35] P. Suetens. *Fundamentals of medical imaging*. Cambridge Univ Pr, 2002.

[36] P.E. TOMOGRAPHY and I. OBJECTS. DIGITAL IMAGING AND COMMUNICATIONS IN MEDICINE (DICOM).

[37] R.L. ValeryNaranjo, P. Paniagua, M. Alcaniz, and S. Albalat. A New Approach in Metal Artifact Reduction for CT 3D Reconstruction? In *Bioinspired Applications in Artificial and Natural Computation: Third International Work-Conference on the Interplay Between Natural and Artificial Computation, Iwinac 2009, Santiago de Compostela, Spain, June 22-26, 2009, Proceedings, Part II*, page 11. Springer-Verlag New York Inc, 2009.

[38] M.W. Vannier. Iterative Deblurring for CT Metal Artifact Reduction. *IEEE TRANSACTIONS ON MEDICAL IMAGING*, 15(5):651, 1996.

[39] M.W. Vannier, C.F. Hildebolt, G. Conover, R.H. Knapp, N. Yokoyama-Crothers, and G. Wang. Three-dimensional dental imaging by spiral CT A progress report. *Oral Surgery, Oral Medicine, Oral Pathology, Oral Radiology and Endodontology*, 84(5):561–570, 1997.

[40] B. Weiss. Fast median and bilateral filtering. In *ACM SIGGRAPH 2006 Papers*, page 526. ACM, 2006.

[41] H. Zaidi, M.L. Montandon, and A. Alavi. Advances in attenuation correction techniques in PET. *PET Clinics*, 2(2):191–217, 2007.

[42] H.K. Zhao, T. Chan, B. Merriman, and S. Osher. A variational level set approach to multiphase motion. *Journal of computational physics*, 127(1):179–195, 1996.